

Universality of Gluon Saturation from Physics-Informed Neural Networks

Wei Kou^{1, 2, 3, 4, *} and Xurong Chen^{1, 2, 3, 4, †}

¹*Institute of Modern Physics, Chinese Academy of Sciences, Lanzhou 730000, Gansu Province, China*

²*Southern Center for Nuclear Science Theory (SCNT), Institute of Modern Physics,*

Chinese Academy of Sciences, Huizhou 516000, Guangdong Province, China

³*School of Nuclear Science and Technology, University of Chinese Academy of Sciences, Beijing 100049, China*

⁴*State Key Laboratory of Heavy Ion Science and Technology, Institute of Modern Physics,*

Chinese Academy of Sciences, Lanzhou 730000, Gansu Province, China

(Dated: January 26, 2026)

The universality of the color dipole amplitude is a cornerstone of high-energy Quantum Chromodynamics (QCD). However, standard phenomenological approaches typically rely on rigid parametric ansatzes and often require ad-hoc geometric adjustments to reconcile inclusive and diffractive measurements. To resolve this tension, we introduce Physics-Informed Neural Networks (PINNs) employing a “Teacher–Student” strategy. The rigorous momentum-space Balitsky-Kovchegov evolution dynamics act as the “Teacher,” constraining the solution manifold, while the network “Student” is refined against inclusive HERA F_2 data. This approach extracts a model-independent dipole amplitude without assuming initial states. Strikingly, we demonstrate that this amplitude—without parameter retuning or geometric rescaling—successfully predicts exclusive J/ψ photoproduction cross-sections. This zero-parameter prediction rigorously confirms the universality of the gluon saturation scale and establishes PINNs as a transformative paradigm for uncovering non-perturbative QCD structures.

Introduction.— Unraveling the multi-dimensional gluonic structure of the proton constitutes a central frontier in high-energy nuclear physics. In the small Bjorken- x regime, the rapid proliferation of gluons creates a dense state of matter governed by non-linear recombination—the Color Glass Condensate (CGC) [1–4]. This transition to saturation is formally encoded in the Balitsky-Kovchegov (BK) equation [5–7], which describes the non-linear rapidity evolution of the universal color-dipole scattering amplitude. While the BK equation provides a rigorous theoretical foundation, extracting the universal dipole amplitude directly from experimental data remains a non-trivial inverse problem, crucial for testing the robustness of the saturation picture.

However, reconciling inclusive (DIS) and exclusive (diffractive) measurements within a unified theoretical framework remains a long-standing challenge. Standard phenomenological approaches [8–10] typically rely on rigid parametric ansatzes and often require ad-hoc geometric adjustments to accommodate diverse datasets [11, 12]. In parallel, machine learning (ML) has emerged as a transformative paradigm in high-energy physics [13–16]. Deep learning techniques have revolutionized the unbiased extraction of Parton Distribution Functions (PDFs) [17, 18], accelerated calculations in Lattice QCD [19, 20], and reconstructed geometries in chromofield [21]. More recently, Physics-Informed Neural Networks (PINNs) [22, 23] have introduced a paradigm shift by embedding physical laws directly into the optimization landscape. This capability makes PINNs uniquely consistent for solving ill-posed inverse problems in QCD thermodynamics and spectroscopy [24, 25], yet their potential to solve non-linear evolution equations in the saturation regime remains largely unexplored.

In this Letter, we resolve this tension by introducing a Physics-Informed Neural Network (PINN) framework that incorporates the rigorous momentum-space BK evolution dynamics directly into the learning process. Unlike traditional fitting methods, our approach employs a “Teacher-Student” strategy (inspired by [26]) where the BK equation constrains the solution manifold while the network refines the amplitude against inclusive HERA F_2 data [27, 28]. Crucially, we demonstrate that this amplitude—without any parameter retuning or geometric rescaling—successfully predicts the differential cross-sections of exclusive J/ψ photoproduction [29, 30]. This zero-parameter prediction provides compelling evidence for the universality of the gluon saturation scale and establishes PINNs as a powerful paradigm for bridging perturbative evolution and non-perturbative hadronic structure.

Methodology and Emergent Dynamics.— The evolution of the color dipole amplitude $N(k, Y)$ is governed by the BK equation [5–7], a non-linear renormalization group equation describing the competition between gluon bremsstrahlung and recombination. In the diffusion approximation, this integro-differential equation reduces to a reaction-diffusion PDE: $\partial_Y N = \bar{\alpha}_s(A_0 N - A_1 \partial_L N + A_2 \partial_L^2 N - N^2)$, where $L = \ln(k^2/\Lambda_{\text{QCD}}^2)$ and the quadratic term enforces the unitarity limit (saturation) [31]. Instead of relying on rigid parametric ansatzes common in phenomenology, we treat the determination of N as a PDE-constrained optimization problem via a fully connected PINN (See Fig. 1). We employ a “Teacher-Student” training strategy: the total loss $\mathcal{L} = \lambda_1 \mathcal{L}_{\text{BK}} + \lambda_2 \mathcal{L}_{F_2} + \lambda_3 \mathcal{L}_{\text{Bound}}$ simultaneously enforces the rigorous scattering kinetics dictated by the BK equation (the Teacher) and anchors the solution to the physi-

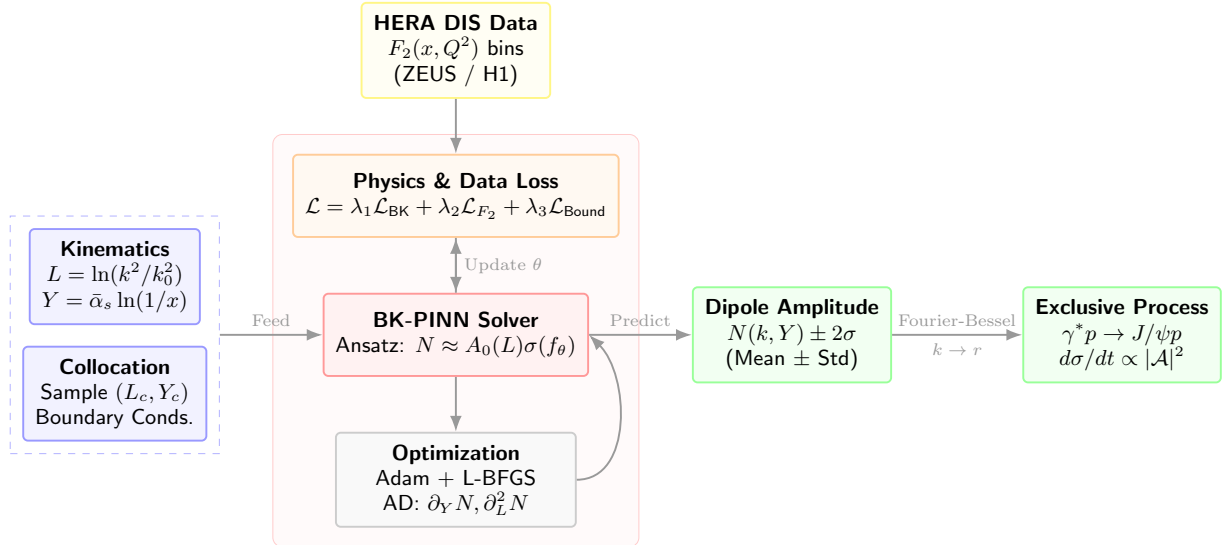


FIG. 1. Workflow of the BK-constrained PINN framework. The training process integrates physical constraints (BK equation) and experimental data (HERA F_2) through a composite loss function. The optimized network yields the momentum-space dipole amplitude $N(k, Y)$, which is then transformed to coordinate space to predict exclusive vector meson production cross-sections.

cal manifold observed by HERA (the Student). This approach allows the network to approximate the dipole amplitude as a universal function approximator, free from ad-hoc model biases.

To bridge the theoretical amplitude with inclusive DIS measurements, we establish a direct link to the structure function $F_2(x, Q^2)$ strictly within momentum space, thereby bypassing the numerical instabilities associated with Fourier-Bessel transforms. Assuming the proton behaves as a homogeneous “black disk” within an effective radius R_p (integrated impact parameter dependence) [32, 33], the structure function is computed via the momentum-space convolution:

$$F_2(x, Q^2) = \frac{Q^2 R_p^2}{2\pi\alpha_{em}} \int_0^1 dz \int \frac{d^2 k}{(2\pi)^2} |\tilde{\Psi}_{\gamma^*}(k, z, Q^2)|^2 N(k, Y), \quad (1)$$

where $\tilde{\Psi}_{\gamma^*}$ denotes the photon wavefunctions (see Appendix). The normalization R_p is the sole geometric parameter determined by the inclusive fit. As shown in Fig. 2, the trained PINN solution spontaneously exhibits geometric scaling [31]—the saturation wavefront propagates towards higher transverse momenta as rapidity increases. It is imperative to emphasize that this scaling behavior was not imposed as an external constraint but emerged naturally from the interplay between the linear growth and non-linear damping terms in the BK equation learned by the network, validating the physical consistency of our framework.

Universality and Zero-Parameter Predictions.— The hallmark of a robust saturation framework lies in its universality—the ability to describe distinct scattering processes with a unified dipole amplitude. We sub-

ject our PINN solution, trained *solely* on inclusive F_2 data, to a rigorous consistency check by predicting the exclusive vector meson photoproduction $\gamma p \rightarrow V p$ ($V = J/\psi, \rho$). The differential cross-section is computed via the standard dipole factorization, $d\sigma/dt \propto (1 + \beta^2) R_p^2 |\int d^2 r \int dz \Psi_V^* \Psi_{\gamma^*} e^{-i\Delta \cdot r} \sigma_{\text{dip}}(r, x)|^2$ (see Appendix for details), where the normalization is fixed by the geometric factor R_p determined in the inclusive fit. Crucially, this calculation involves PINN solution without free parameters, serving as a blind test of the ex-

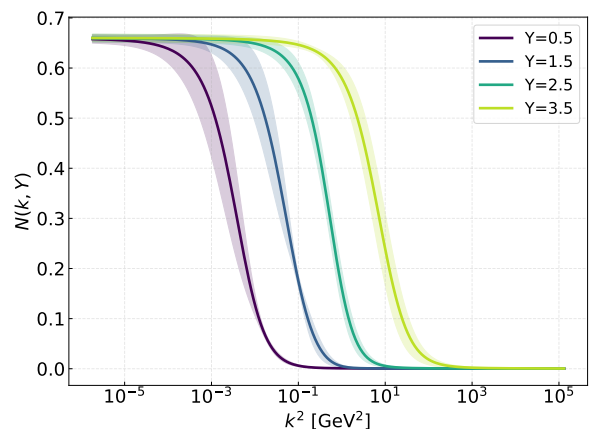


FIG. 2. Evolution of the extracted momentum-space dipole amplitude $N(k, Y)$ with rapidity Y . The curves show the solution at $Y = 0.5, 1.5, 2.5, 3.5$ (from left to right). The wavefront propagation towards higher k^2 illustrates the dynamic generation of the saturation scale $Q_s(Y)$, an emergent property of the PINN solution.

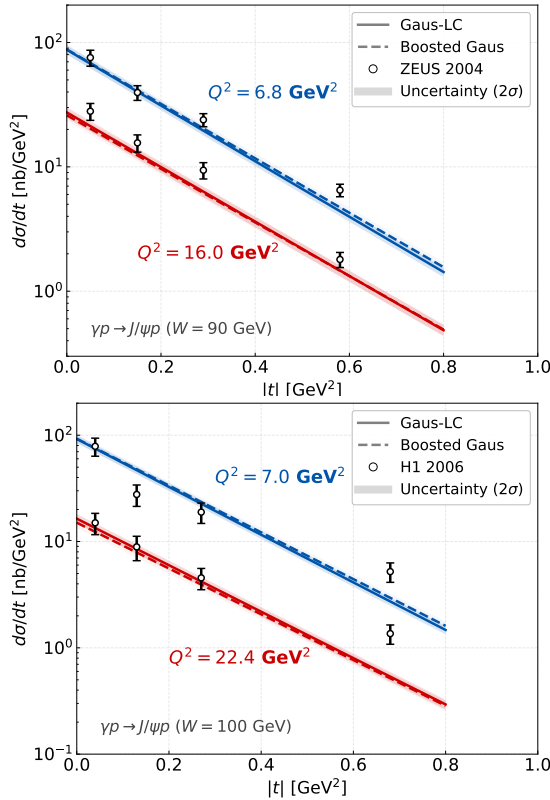


FIG. 3. Zero-parameter predictions for exclusive J/ψ photoproduction. Top: Comparison with ZEUS data at $W = 90$ GeV [29]. Bottom: Comparison with H1 data at $W = 100$ GeV [30]. The solid and dashed lines represent predictions using Gaus-LC and Boosted Gaussian wavefunctions, respectively. The agreement validates the universality of the PINN-extracted amplitude.

tracted gluon dynamics.

Figure 3 presents the comparison between our predictions and HERA measurements for J/ψ production [29, 30]. The agreement is striking: the PINN-derived amplitude not only reproduces the absolute magnitude of the cross-section but, more importantly, accurately captures the diffractive slope (t -dependence) across a wide range of photon virtualities ($6.8 \leq Q^2 \leq 22.4$ GeV^2). Since the t -slope encodes the transverse spatial distribution of gluons, this agreement confirms that the effective geometric profile learned implicitly from inclusive kinematics is consistent with the spatial imaging probed by diffraction. We note that this universality also holds for lighter mesons such as ρ^0 (The type of vector meson does not affect the dipole amplitude.). To quantify the epistemic uncertainty of our predictions, we employ a Bootstrap Aggregating (Bagging) strategy [17, 34, 35]. By training an ensemble of independent PINNs on resampled datasets, we construct a probability distribution of solutions; the resulting error bands (Fig. 3) serve as a frequentist proxy for Bayesian inference, reflecting the

model's confidence in the extrapolated kinematic regions.

Conclusion.— In summary, we have established a unified description of high-energy scattering by integrating the rigorous momentum-space BK evolution dynamics into a Physics-Informed Neural Network. This framework effectively bridges the gap between perturbative QCD evolution and non-perturbative hadronic structure, resolving the long-standing tension between inclusive and diffractive measurements without ad-hoc geometric adjustments. The successful zero-parameter prediction of exclusive J/ψ photoproduction serves as a definitive validation of the universality of the color dipole amplitude. By allowing the geometric scaling properties to emerge naturally from the interplay between the governing equation and inclusive data, our approach confirms that the gluon saturation mechanism is an intrinsic, process-independent feature of the proton's high-energy wave function.

While the current results are compelling, the framework opens clear avenues for systematic refinement. The validity of the diffusion approximation restricts the current applicability to a specific kinematic window; future iterations will incorporate full next-to-leading order (NLO) corrections and explicit impact-parameter dependence to extend precision across a broader Q^2 range. Furthermore, the integration of advanced machine learning architectures, such as Bayesian Neural Networks (BNNs) [36, 37] for rigorous uncertainty quantification and Operator Learning for parameter-dependent solutions, will be essential for maximizing the discovery potential of future high-precision data from the Electron-Ion Collider (EIC) [38, 39]. Ultimately, this work demonstrates that physics-informed deep learning is not merely a fitting tool, but a transformative paradigm for uncovering the fundamental laws of strong interaction.

This work has been supported by the National Natural Science Foundation of China (Grant No. 12547118), the Research Program of State Key Laboratory of Heavy Ion Science and Technology, Institute of Modern Physics, Chinese Academy of Sciences (Grant No. HIST2025CS08), and the National Key R&D Program of China (Grant No. 2024YFE0109800 and 2024YFE0109802).

* kouwei@impcas.ac.cn

† xchen@impcas.ac.cn

- [1] L. V. Gribov, E. M. Levin, and M. G. Ryskin, Semihard Processes in QCD, *Phys. Rept.* **100**, 1 (1983).
- [2] A. H. Mueller and J.-w. Qiu, Gluon Recombination and Shadowing at Small Values of x , *Nucl. Phys. B* **268**, 427 (1986).
- [3] L. D. McLerran and R. Venugopalan, Computing quark and gluon distribution functions for very large nuclei, *Phys. Rev. D* **49**, 2233 (1994), [arXiv:hep-ph/9309289](https://arxiv.org/abs/hep-ph/9309289).

[4] F. Gelis, E. Iancu, J. Jalilian-Marian, and R. Venugopalan, The Color Glass Condensate, *Ann. Rev. Nucl. Part. Sci.* **60**, 463 (2010), arXiv:1002.0333 [hep-ph].

[5] I. Balitsky, Operator expansion for high-energy scattering, *Nucl. Phys. B* **463**, 99 (1996), arXiv:hep-ph/9509348.

[6] Y. V. Kovchegov, Unitarization of the BFKL pomeron on a nucleus, *Phys. Rev. D* **61**, 074018 (2000), arXiv:hep-ph/9905214.

[7] Y. V. Kovchegov, Small x F(2) structure function of a nucleus including multiple pomeron exchanges, *Phys. Rev. D* **60**, 034008 (1999), arXiv:hep-ph/9901281.

[8] K. J. Golec-Biernat and M. Wusthoff, Saturation effects in deep inelastic scattering at low Q^{**2} and its implications on diffraction, *Phys. Rev. D* **59**, 014017 (1998), arXiv:hep-ph/9807513.

[9] E. Iancu, K. Itakura, and S. Munier, Saturation and BFKL dynamics in the HERA data at small x, *Phys. Lett. B* **590**, 199 (2004), arXiv:hep-ph/0310338.

[10] H. Kowalski, L. Motyka, and G. Watt, Exclusive diffractive processes at HERA within the dipole picture, *Phys. Rev. D* **74**, 074016 (2006), arXiv:hep-ph/0606272.

[11] H. Kowalski and D. Teaney, An Impact parameter dipole saturation model, *Phys. Rev. D* **68**, 114005 (2003), arXiv:hep-ph/0304189.

[12] H. Mäntysaari and B. Schenke, Revealing proton shape fluctuations with incoherent diffraction at high energy, *Phys. Rev. D* **94**, 034042 (2016), arXiv:1607.01711 [hep-ph].

[13] D. Guest, K. Cranmer, and D. Whiteson, Deep Learning and its Application to LHC Physics, *Ann. Rev. Nucl. Part. Sci.* **68**, 161 (2018), arXiv:1806.11484 [hep-ex].

[14] A. Radovic, M. Williams, D. Rousseau, M. Kagan, D. Bonacorsi, A. Himmel, A. Aurisano, K. Terao, and T. Wongjirad, Machine learning at the energy and intensity frontiers of particle physics, *Nature* **560**, 41 (2018).

[15] A. Boehnlein *et al.*, Colloquium: Machine learning in nuclear physics, *Rev. Mod. Phys.* **94**, 031003 (2022), arXiv:2112.02309 [nucl-th].

[16] K. Zhou, L. Wang, L.-G. Pang, and S. Shi, Exploring QCD matter in extreme conditions with Machine Learning, *Prog. Part. Nucl. Phys.* **135**, 104084 (2024), arXiv:2303.15136 [hep-ph].

[17] R. D. Ball *et al.* (NNPDF), Parton distributions from high-precision collider data, *Eur. Phys. J. C* **77**, 663 (2017), arXiv:1706.00428 [hep-ph].

[18] S. Carrazza and J. Cruz-Martinez, Towards a new generation of parton densities with deep learning models, *Eur. Phys. J. C* **79**, 676 (2019), arXiv:1907.05075 [hep-ph].

[19] P. Shanahan *et al.*, Snowmass 2021 Computational Frontier CompF03 Topical Group Report: Machine Learning, (2022), arXiv:2209.07559 [physics.comp-ph].

[20] S. Shi, K. Zhou, J. Zhao, S. Mukherjee, and P. Zhuang, From lattice QCD to in-medium heavy-quark interactions via deep learning, *PoS LATTICE2021*, 537 (2022).

[21] W. Kou and X. Chen, Machine learning insights into quark-antiquark interactions: probing field distributions and string tension in QCD, *Eur. Phys. J. C* **85**, 261 (2025), arXiv:2411.14902 [hep-ph].

[22] M. Raissi, P. Perdikaris, and G. E. Karniadakis, Physics-informed neural networks: A deep learning framework for solving forward and inverse problems involving nonlinear partial differential equations, *J. Comput. Phys.* **378**, 686 (2019), arXiv:1711.10561 [cs.AI].

[23] G. E. Karniadakis, I. G. Kevrekidis, L. Lu, P. Perdikaris, S. Wang, and L. Yang, Physics-informed machine learning, *Nature Reviews Physics* **3**, 422 (2021).

[24] G. Aarts, K. Fukushima, T. Hatsuda, A. Ipp, S. Shi, L. Wang, and K. Zhou, Physics-driven learning for inverse problems in quantum chromodynamics, *Nature Rev. Phys.* **7**, 154 (2025), arXiv:2501.05580 [hep-lat].

[25] W. Kou, X. Lin, B. Guo, and X. Chen, Physics-informed neural network approach to quark-antiquark color flux tube, *Phys. Rev. D* **112**, 056027 (2025), arXiv:2506.03513 [hep-ph].

[26] Z. Liu, Y. Liu, X. Yan, W. Liu, H. Nie, S. Guo, and C.-a. Zhang, Automatic network structure discovery of physics informed neural networks via knowledge distillation, *Nature Communications* **16**, 9558 (2025).

[27] F. D. Aaron *et al.* (H1, ZEUS), Combined Measurement and QCD Analysis of the Inclusive e+ - p Scattering Cross Sections at HERA, *JHEP* **01**, 109, arXiv:0911.0884 [hep-ex].

[28] V. Andreev *et al.* (H1), Measurement of inclusive ep cross sections at high Q^2 at $\sqrt{s} = 225$ and 252 GeV and of the longitudinal proton structure function F_L at HERA, *Eur. Phys. J. C* **74**, 2814 (2014), arXiv:1312.4821 [hep-ex].

[29] S. Chekanov *et al.* (ZEUS), Exclusive electroproduction of J/psi mesons at HERA, *Nucl. Phys. B* **695**, 3 (2004), arXiv:hep-ex/0404008.

[30] A. Aktas *et al.* (H1), Elastic J/psi production at HERA, *Eur. Phys. J. C* **46**, 585 (2006), arXiv:hep-ex/0510016.

[31] S. Munier and R. B. Peschanski, Geometric scaling as traveling waves, *Phys. Rev. Lett.* **91**, 232001 (2003), arXiv:hep-ph/0309177.

[32] X. Wang, W. Kou, G. Xie, Y.-P. Xie, and X. Chen, Exclusive vector meson production with the analytical solution of Balitsky-Kovchegov equation, *Chin. Phys. C* **46**, 093101 (2022), arXiv:2205.02396 [hep-ph].

[33] X.-Y. Wang, C. Dong, and X. Liu, Analysis of Strong Coupling Constant with Machine Learning and Its Application, *Chin. Phys. Lett.* **41**, 031201 (2023), arXiv:2304.07682 [hep-ph].

[34] B. Efron, Bootstrap Methods: Another Look at the Jackknife, *Annals Statist.* **7**, 1 (1979).

[35] B. Lakshminarayanan, A. Pritzel, and C. Blundell, Simple and scalable predictive uncertainty estimation using deep ensembles (2017), arXiv:1612.01474 [stat.ML].

[36] R. M. Neal, *Bayesian learning for neural networks*, Vol. 118 (Springer Science & Business Media, 2012).

[37] L. V. Jospin, H. Laga, F. Boussaid, W. Buntine, and M. Bennamoun, Hands-on bayesian neural networks—a tutorial for deep learning users, *IEEE Computational Intelligence Magazine* **17**, 29–48 (2022).

[38] A. Accardi *et al.*, Electron Ion Collider: The Next QCD Frontier: Understanding the glue that binds us all, *Eur. Phys. J. A* **52**, 268 (2016), arXiv:1212.1701 [nucl-ex].

[39] R. Abdul Khalek *et al.*, Science Requirements and Detector Concepts for the Electron-Ion Collider: EIC Yellow Report, *Nucl. Phys. A* **1026**, 122447 (2022), arXiv:2103.05419 [physics.ins-det].

Supplemental Material for:
Unveiling the Universality of Gluon Saturation via Physics-Informed Neural Networks

Theoretical Formalism

A. Momentum-Space BK Equation in Diffusion Approximation

The evolution of the dipole scattering amplitude $N(k, Y)$ in momentum space is governed by the BK equation. In the diffusion approximation, the non-linear integro-differential equation can be simplified to a partial differential equation (PDE). By expanding the BFKL kernel $\chi(\gamma)$ around the saddle point $\gamma = 1/2$, the equation takes the form [31, 32]:

$$\frac{\partial N(L, Y)}{\partial Y} = \bar{\alpha}_s [\chi(-\partial_L)N - N^2], \quad (\text{S1})$$

where $Y = \ln(1/x)$ is the rapidity, $L = \ln(k^2/\Lambda_{\text{QCD}}^2)$ is the logarithmic transverse momentum, and $\bar{\alpha}_s = \alpha_s N_c/\pi$. In the diffusion limit, the kernel operator is approximated as:

$$\chi(-\partial_L) \approx A_0 - A_1 \partial_L + A_2 \partial_L^2. \quad (\text{S2})$$

Consequently, the PDE constraint used in our PINN (\mathcal{L}_{PDE}) is explicitly written as:

$$\frac{\partial N}{\partial Y} = \bar{\alpha}_s \left(A_0 N - A_1 \frac{\partial N}{\partial L} + A_2 \frac{\partial^2 N}{\partial L^2} - N^2 \right). \quad (\text{S3})$$

The coefficients are derived from the BFKL characteristic function: $A_0 = \chi(1/2) = 4 \ln 2$, $A_1 = 0$ (in the symmetric frame), and $A_2 = \chi''(1/2)/2 = 14\zeta(3)$. In this work, we use these standard values to enforce the physical evolution.

B. Inclusive Structure Function F_2

To directly utilize the momentum-space output of our PINN, the inclusive proton structure function $F_2(x, Q^2)$ is computed via the convolution of the momentum-space photon wavefunctions and the dipole amplitude. The explicit expression is given by

$$F_2(x, Q^2) = \frac{Q^2 R_p^2}{2\pi\alpha_{em}} \int_0^1 dz \int \frac{d^2 k}{(2\pi)^2} |\tilde{\Psi}_{\gamma^*}(k, z, Q^2)|^2 N(k, Y), \quad (\text{S4})$$

Here, $|\tilde{\Psi}_{\gamma}|^2$ represents the squared photon wave function summed over flavors f . In momentum space, incorporating massive quarks ($\bar{Q}_f^2 = z(1-z)Q^2 + m_f^2$), it takes the form:

$$\begin{aligned} \left| \tilde{\Psi}_{\gamma}(k^2, z; Q^2) \right|^2 &= \sum_f \left(\frac{4\bar{Q}_f^2}{k^2 + 4\bar{Q}_f^2} \right)^2 e_f^2 \left\{ [z^2 + (1-z)^2] \right. \\ &\quad \times \left[\frac{4(k^2 + \bar{Q}_f^2)}{\sqrt{k^2(k^2 + 4\bar{Q}_f^2)}} \operatorname{arcsinh} \left(\frac{k}{2\bar{Q}_f} \right) + \frac{k^2 - 2\bar{Q}_f^2}{2\bar{Q}_f^2} \right] \\ &\quad + \frac{4Q^2 z^2 (1-z)^2 + m_f^2}{\bar{Q}_f^2} \\ &\quad \times \left. \left[\frac{k^2 + \bar{Q}_f^2}{\bar{Q}_f^2} - \frac{4\bar{Q}_f^4 + 2\bar{Q}_f^2 k^2 + k^4}{\bar{Q}_f^2 \sqrt{k^2(k^2 + 4\bar{Q}_f^2)}} \operatorname{arcsinh} \left(\frac{k}{2\bar{Q}_f} \right) \right] \right\}. \end{aligned} \quad (\text{S5})$$

This formulation allows for a direct evaluation of inclusive observables from the momentum-space solution $N(k, Y)$ without intermediate coordinate-space transformations during the training phase.

Exclusive Vector Meson Production

To validate the universality of the extracted amplitude, we calculate the exclusive production of J/ψ mesons. Following Ref. [32], the scattering amplitude for $\gamma^* p \rightarrow V p$ is given by:

$$\mathcal{A}_{T,L}(x, Q^2, \Delta) = i \int d^2 \mathbf{r} \int_0^1 dz (\Psi_V^* \Psi_{\gamma^*})_{T,L} \cdot \sigma_{\text{dip}}(r, x) \cdot e^{-i\Delta \cdot \mathbf{b}}. \quad (\text{S6})$$

Assuming a factorized dependence on the impact parameter b , the integration over b yields the diffractive slope factor $e^{-B_D|t|/2}$. For this exclusive process, we map the PINN's momentum-space output to coordinate space via the Hankel transform:

$$\sigma_{\text{dip}}(r, x) = 2\pi R_p^2 \int_0^\infty k dk J_0(kr) N(k, Y). \quad (\text{S7})$$

A. Differential Cross Sections

The differential cross-section is expressed as:

$$\frac{d\sigma}{dt} = \frac{1}{16\pi} (1 + \beta^2) R_g^2 (|\mathcal{A}_T|^2 + |\mathcal{A}_L|^2), \quad (\text{S8})$$

where β accounts for the real part of the scattering amplitude and R_g is the skewedness correction factor arising from the difference between diagonal and off-diagonal gluon distributions. Assuming a local power-law dependence of the amplitude $\mathcal{A} \propto (1/x)^\lambda$, these factors are analytic functions of λ :

$$\beta = \tan\left(\frac{\pi\lambda}{2}\right), \quad R_g = \frac{2^{2\lambda+3}}{\sqrt{\pi}} \frac{\Gamma(\lambda + 5/2)}{\Gamma(\lambda + 4)}. \quad (\text{S9})$$

In our calculations, we use an effective λ derived from the saturation exponent consistent with our extracted parameters.

B. Wavefunction Overlap

We use two standard wavefunction parameterizations [10]:

- Gaus-LC: $\phi(r, z) \propto z(1-z) \exp(-r^2/2R^2)$.
- Boosted Gaussian: $\phi(r, z) \propto z(1-z) \exp\left(-\frac{m_f^2 \mathcal{R}^2}{8z(1-z)} - \frac{2z(1-z)r^2}{\mathcal{R}^2}\right)$.

PINN Training Strategy

A. Network Architecture

We employ a fully connected neural network (FCNN) to approximate the dipole amplitude $N(L, Y)$. The detailed architecture is illustrated in Fig. S1. The network consists of:

- Input Layer: Accepts the logarithmic transverse momentum $L = \ln(k^2/\Lambda_{\text{QCD}}^2)$ and rapidity $Y = \ln(1/x)$.
- Hidden Layers: Four fully connected layers, each containing 64 neurons. We use the hyperbolic tangent (\tanh) as the activation function for all hidden layers to ensure the smoothness required for computing high-order derivatives in the PDE loss.
- Output Layer: A single neuron with a Sigmoid activation function $\sigma(x) = 1/(1 + e^{-x})$, strictly constraining the output amplitude to the physical unitarity limit $0 < N < 1$.

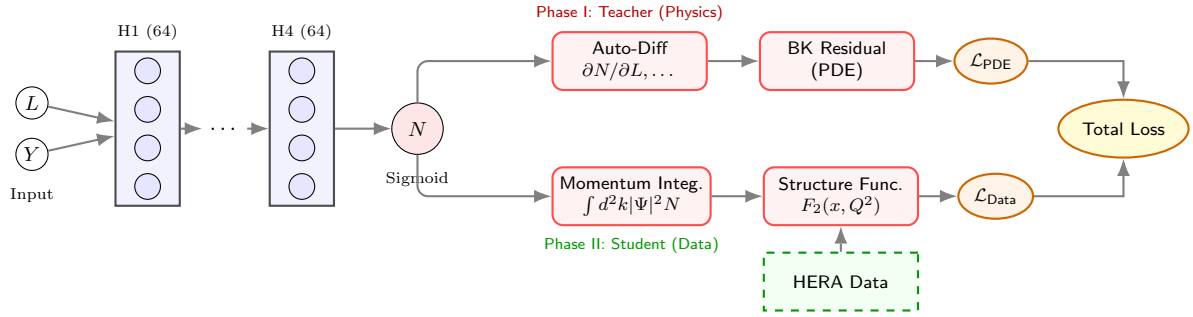


FIG. S1. Schematic of the BK-PINN architecture. The network maps kinematic inputs (L, Y) to the momentum-space dipole amplitude N . The training is governed by two loss components: the physics-based \mathcal{L}_{PDE} derived from the BK equation via automatic differentiation, and the data-driven $\mathcal{L}_{\text{Data}}$ obtained by directly integrating the amplitude with photon wavefunctions in momentum space to match HERA F_2 data.

B. Teacher-Student Strategy

We employ a two-phase “Teacher-Student” training strategy to ensure physical consistency:

- Phase I (Teacher): The network is trained solely on the PDE loss \mathcal{L}_{PDE} (Eq. S3). This enforces the BK evolution dynamics, acting as a “teacher” to establish the physical manifold of the solution before seeing data.
- Phase II (Student): The data loss $\mathcal{L}_{\text{Data}}$ (from HERA F_2) is activated. The network (“student”) refines the solution to match experimental observations while remaining constrained by the physics learned in Phase I.

C. Data Splitting and Uncertainty Quantification

The HERA F_2 dataset is randomly partitioned into a training set (80%) and a testing set (20%). To quantify epistemic uncertainty, we use the Bootstrap Aggregating (Bagging) method. We train an ensemble of $N = 20$ independent PINNs on resampled datasets. The final prediction is the ensemble mean, and the uncertainty band corresponds to $\pm 2\sigma$ (standard deviation).

S-IV. Statistical Validation and Results

Loss Convergence

Figure S2 shows the loss history. Note the initial drop in PDE loss followed by the synchronous convergence of data losses.

Statistical Analysis

To assess the quality of the PINN fit, we perform a statistical analysis of the residuals. Figure S3 compares the predicted F_2 values (ensemble mean) against the experimental data. The points cluster tightly around the diagonal $y = x$ line. Figure S4 displays the distribution of the pull variable, $(F_2^{\text{pred}} - F_2^{\text{data}})/\sigma_{\text{data}}$. The distribution approximates a standard normal Gaussian ($\mu \approx 0, \sigma \approx 1$), indicating that the model provides an unbiased description of the data within experimental uncertainties.

Inclusive Fit Result

The resulting fit to the F_2 structure function is shown in Fig. S5.

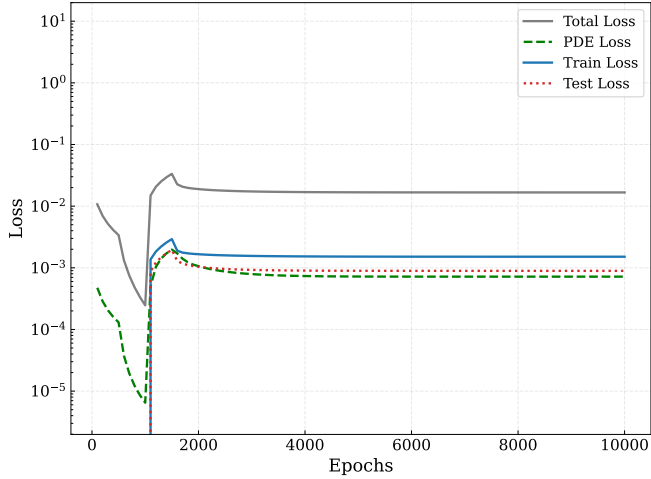


FIG. S2. Training dynamics showing the total loss, PDE loss (Teacher), and Data loss (Student) for both training and testing sets.

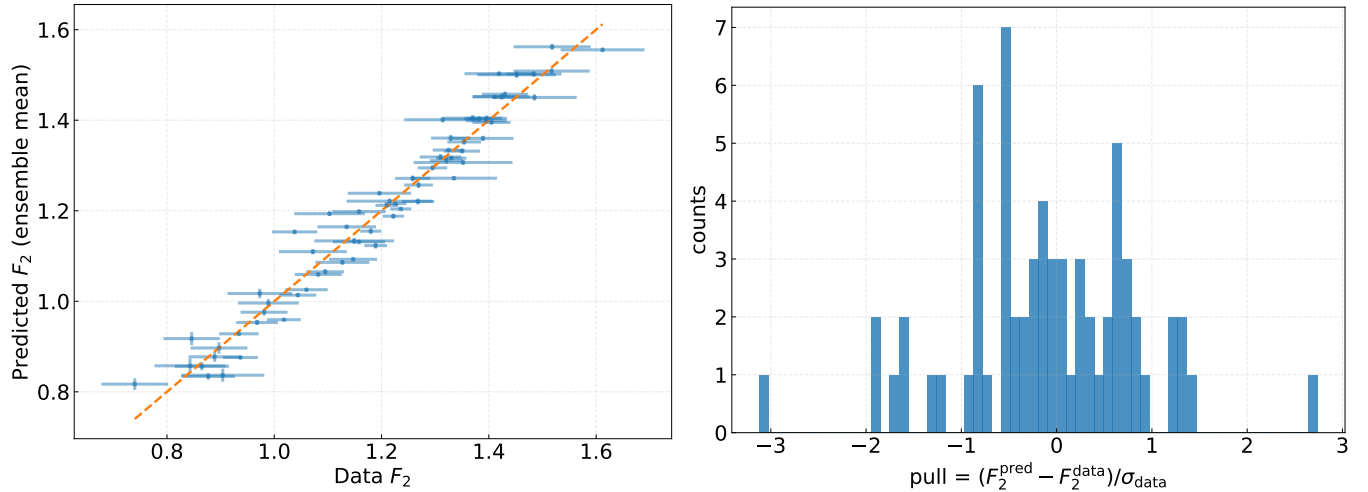


FIG. S3. Parity plot of predicted vs. experimental F_2 .

FIG. S4. Pull distribution of the residuals.

S-V. Extracted Parameters and Physical Interpretation

A key advantage of the PINN framework is its ability to extract the underlying parameters of the governing equation from data. We analyze the ensemble of trained networks to infer the effective coefficients of the BK equation in the diffusion approximation.

Table S1 summarizes the mean values and standard deviations of the extracted parameters. Here, A_1 represents the corrected drift coefficient ($0.191 \times A_1$) learned by the network.

TABLE S1. Mean values and standard deviations of the parameters extracted from the PINN ensemble.

Parameter	Symbol	Mean	Std
Intercept/Growth	A_0	0.661	0.004
Drift Coefficient (Corrected)	A_1	0.414	0.013
Diffusion Coefficient	A_2	0.266	0.033
Proton Radius Parameter	R_p [GeV $^{-1}$]	5.456	0.0004

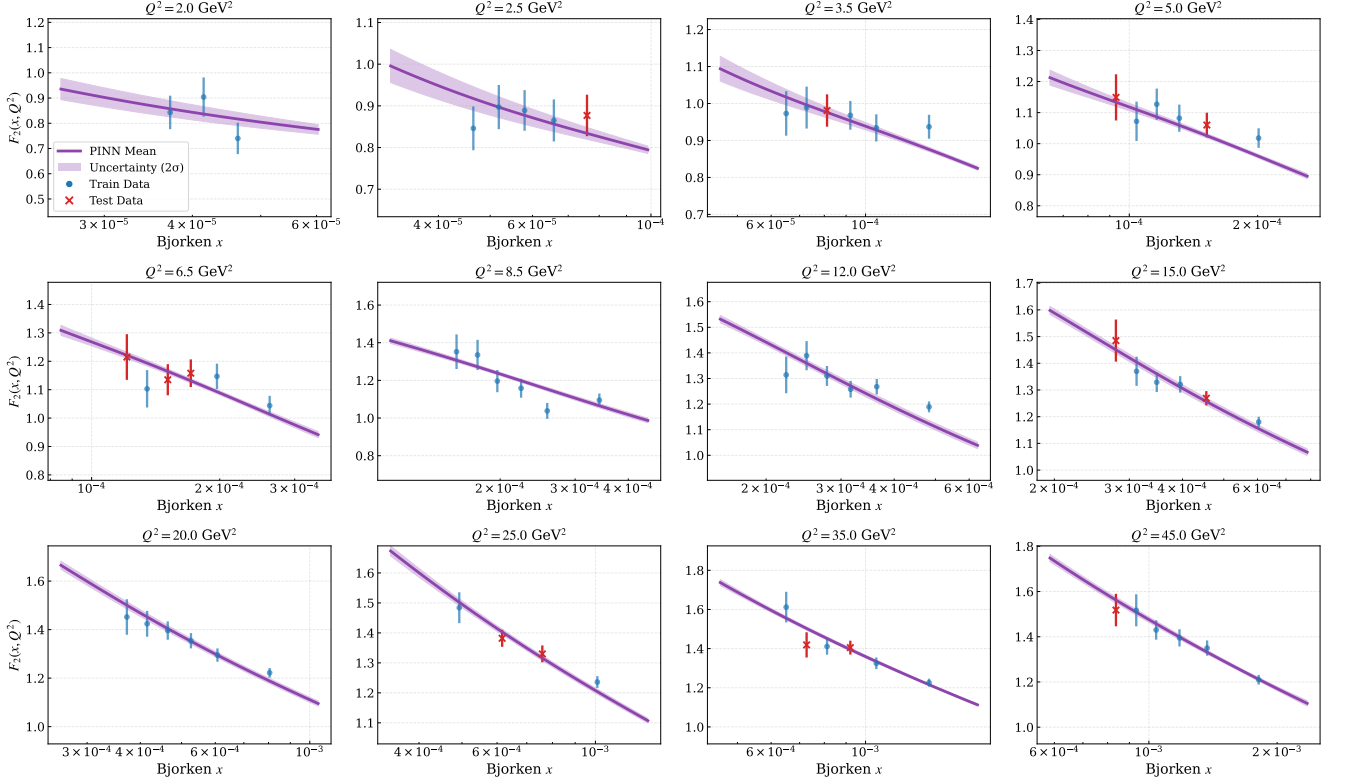


FIG. S5. PINN fit to inclusive F_2 data. The shaded bands represent the 2σ uncertainty derived from the ensemble.

Saturation Exponent λ_s

The saturation scale $Q_s^2(x)$ characterizes the onset of non-linear effects and is expected to grow as a power of $1/x$: $Q_s^2(x) \propto (1/x)^{\lambda_s}$. In the traveling wave solution of the BK equation, the saturation exponent is related to the wave velocity v by $\lambda_s = v\bar{\alpha}_s$. The wave velocity is determined by the linear parameters of the equation:

$$v = A_1 + 2\sqrt{A_0 A_2}. \quad (\text{S10})$$

Using the extracted parameters and a fixed coupling constant $\bar{\alpha}_s = 0.191$, we derive:

$$v \approx 1.251 \pm 0.054. \quad (\text{S11})$$

This yields a saturation exponent of:

$$\lambda_s = v\bar{\alpha}_s \approx 0.239 \pm 0.010. \quad (\text{S12})$$

This result is in remarkable agreement with phenomenological extractions from HERA data, where λ_s is typically found to be in the range of $0.20 \sim 0.30$ (e.g., $\lambda \approx 0.288$ in the GBW model). The fact that our PINN autonomously converges to this physical value confirms that it has correctly captured the energy evolution dynamics of the gluon density.

Proton Radius

The extracted normalization parameter $R_p \approx 5.46 \text{ GeV}^{-1}$ corresponds to $R_p \approx 1.07 \text{ fm}$. It is crucial to clarify that this value does not represent the electromagnetic charge radius of the free proton ($r_E \approx 0.84 \text{ fm}$). Instead, R_p in the dipole factorization framework represents an effective transverse radius characterizing the spatial extent of the gluon distribution involved in the scattering process. Unlike the valence-quark dominated charge radius, the gluonic radius is expected to grow with decreasing Bjorken- x due to Gribov diffusion. The extracted value is consistent with the diffractive slope parameter B_D measured at HERA, reflecting the “black disk” limit of the proton at high energies.

S-VI. Total Cross Section

To further verify the predictive power of our model, we calculate the total cross-section for exclusive J/ψ photoproduction as a function of Q^2 . The total cross-section is obtained by integrating the differential cross-section over the momentum transfer t . Given the exponential dependence $d\sigma/dt \sim e^{-B|t|}$, this can be approximated as $\sigma_{\text{tot}} \approx \frac{1}{B} \frac{d\sigma}{dt}|_{t=0}$.

Figure S6 shows the PINN predictions using both Gaus-LC (solid red) and Boosted Gaussian (dashed green) wavefunctions at a fixed center-of-mass energy $W = 90$ GeV. We compare our zero-parameter predictions with experimental data from ZEUS 2004 [29] and H1 2006 [30]. The model successfully reproduces the Q^2 dependence of the cross-section over three orders of magnitude ($0.05 \lesssim Q^2 \lesssim 100$ GeV 2). This agreement confirms that the dipole amplitude extracted from inclusive data correctly encodes the scale dependence required to describe exclusive observables, further validating the universality of the saturation mechanism captured by the PINN.

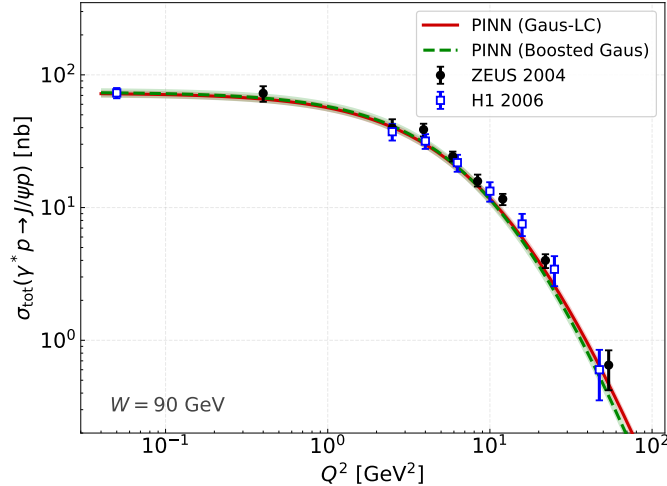


FIG. S6. Total cross section σ_{tot} for exclusive J/ψ photoproduction as a function of Q^2 at fixed center-of-mass energy $W = 90$ GeV. The PINN predictions using Gaus-LC (red solid) and Boosted Gaussian (green dashed) wavefunctions are compared with experimental data from ZEUS 2004 [29] and H1 2006 [30]. The shaded bands indicate the 2σ uncertainty.